SPECIAL FEATURE: PERSPECTIVE

Metal halide perovskite light emitters

Young-Hoon Kim[a,b,1], Himchan Cho[a,b,1], and Tae-Woo Lee[a,b,2]

Edited by John A. Rogers, University of Illinois, Urbana, IL, and approved August 16, 2016 (received for review May 10, 2016)

Twenty years after layer-type metal halide perovskites were successfully developed, 3D metal halide perovskites (shortly, perovskites) were recently rediscovered and are attracting multidisciplinary interest from physicists, chemists, and material engineers. Perovskites have a crystal structure composed of five atoms per unit cell (ABX_3) with cation A positioned at a corner, metal cation B at the center, and halide anion X at the center of six planes and unique optoelectronic properties determined by the crystal structure. Because of very narrow spectra (full width at half-maximum ≤20 nm), which are insensitive to the crystallite/grain/particle dimension and wide wavelength range (400 nm ≤ λ ≤ 780 nm), perovskites are expected to be promising high-color purity light emitters that overcome inherent problems of conventional organic and inorganic quantum dot emitters. Within the last 2 y, perovskites have already demonstrated their great potential in light-emitting diodes by showing high electroluminescence efficiency comparable to those of organic and quantum dot light-emitting diodes. This article reviews the progress of perovskite emitters in two directions of bulk perovskite polycrystalline films and perovskite nanoparticles, describes current challenges, and suggests future research directions for researchers to encourage them to collaborate and to make a synergetic effect in this rapidly emerging multidisciplinary field.

organic–inorganic hybrid perovskite | light-emitting diodes | polycrystalline film | nanoparticle | vivid display

As human civilization went through the information revolution, display technology has been designated as a core technology to increase convenience in daily human life. In an information society, the desire of humans to see the materials more vividly in displays has significantly increased. In this aspect, major trend of the display technology is changing from high resolution and high efficiency to high color purity for realizing vivid natural colors (Fig. 1). Therefore, research on new emitting materials that can emit light with narrow full width at half-maximum (FWHM) have been attempted. Inorganic quantum dot (QD) emitters with narrow spectra (FWHM ~30 nm) have been significantly studied following organic emitters (FWHM >40 nm); however, size-sensitive color purity, difficult size uniformity control, and expensive material costs of inorganic QD emitters retard the progress for wide use in industry. Therefore, new emitters with size-insensitively high color purity (FWHM <20 nm) and low material cost should be developed. Among many candidates, metal halide perovskites (hereafter, "perovskites") have gained great attentions and shown the possibility for future high-color purity emitters.

The first perovskites were layer-type thin films (A_2MX_4) (A = organic cation; M = divalent metal; X = Cl, Br, I) (1–6). They were expected to be novel hybrid materials that had both advantages of organic materials (e.g., solution processability and low material costs) and inorganic materials (e.g., high charge carrier mobility) (7). Especially, perovskites with high color purity, easy wavelength tuning, and efficient charge injection/transport property have been intensively studied as promising candidates for future light emitters (8–10). Furthermore, stable and environmentally benign perovskites, which were recently reported, further raise the possibility of perovskites as future emitters in display technology (11–19).

However, early works on layer-type (i.e., 2D) perovskite emitters, in the 1990s, did not gain much attention (1–5). The layer-type perovskite emitters incorporating long-chain organic ammoniums can generate stable excitons at low temperature, but the photoluminescence (PL) intensity dramatically decreased as temperature increased, so the perovskite light-emitting diodes (PeLEDs) exhibited electroluminescence (EL) only at low temperature (<110 K) (1–5). The PeLEDs that exhibited EL at room temperature (RT) were first fabricated in 1999 using a layer-type perovskite incorporating an organic dye molecule ($H_2NC_2H_4C_{16}H_8S_4$–$C_2H_4NH_2$) and exhibited a maximum

[a]Department of Materials Science and Engineering, Pohang University of Science and Technology, Pohang, Gyungbuk 790-784, Republic of Korea; and [b]Department of Materials Science and Engineering, Seoul National University, Gwanak-gu, Seoul 08826, Republic of Korea

Author contributions: Y.-H.K., H.C., and T.-W.L. wrote the paper.

The authors declare no conflict of interest.

This article is a PNAS Direct Submission.

[1]Y.-H.K. and H.C. contributed equally to this work.

[2]To whom correspondence should be addressed. Email: twlees@snu.ac.kr.

www.pnas.org/cgi/doi/10.1073/pnas.1607471113

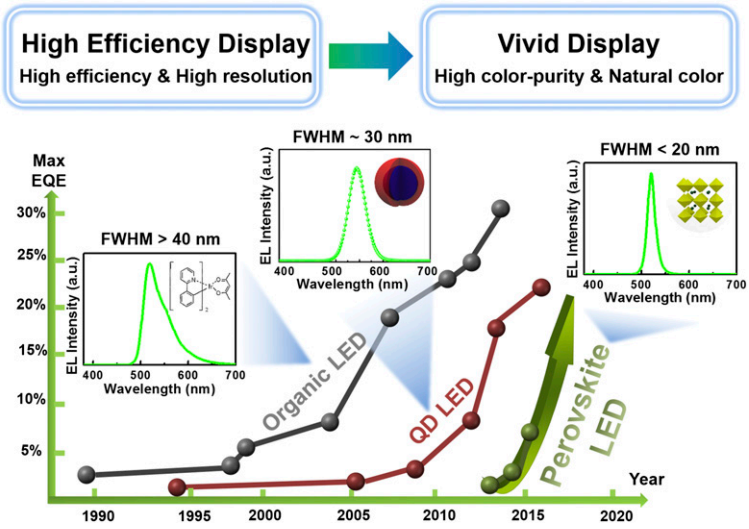

Fig. 1. Major trend of display technology. Data are taken from references as follows: OLEDs, refs. 30–41; QD LEDs, refs. 20–29; and PeLEDs, refs. 8–10.

external quantum efficiency (EQE_{max}) of 0.11% (7). However, this emission originated not from the inorganic frameworks but from the organic dye ligands; thus, PeLEDs showed very low color purity (FWHM ≥ 100 nm) compared with inorganic QD LEDs (20–29), and inferior EL efficiency compared with organic LEDs (OLEDs) (30–41). As a result, the development of these perovskite emitters has been retarded, whereas organic emitters and inorganic QD emitters have been intensively studied for 27 y and 22 y, respectively (20–41).

In 2012, the first 3D perovskite emitters, $CH_3NH_3PbBr_3$ nanoparticles (NPs) in porous alumina (42), were reported, and the possibility of perovskites as emitters was rediscovered. As a result, since 2014, the research on 3D perovskite emitters has intensively grown and focused on achieving high efficiency in PL and EL. Within the last 2 y, more than 72 papers on perovskite emitters were published, and EQE_{max} of 8.53% and photoluminescence quantum efficiency (PLQE) of more than 90% were reported (10, 43).

In this Perspective, we highlight the potential of perovskites as promising emitters that can be mainstream in the research field of displays and solid-state lightings. In addition, we present our perspectives on the progress of perovskite emitters in two directions: bulk perovskite polycrystalline films (PePCs) and perovskite nanoparticles (PeNPs). Finally, we suggest future research directions of perovskite emitters that may engage a researcher's attention in this research field.

Fundamental Properties of Perovskite Emitters

Three-dimensional perovskites have an ABX_3 crystal structure composed of five atoms per unit cell, with cation A positioned at a corner, metal cation B at the center, and six nearest-neighbor anions X with octahedral corner sharing at the center of six planes (Fig. 2*A*). Generally, perovskites consist of organic ammonium ($C_nH_{2n}{}^{+1}NH_3{}^{+}$) or organic amidinium [e.g., $CH(NH_2)^+$] or alkali metals such as Cs at the A site, divalent transition metals (e.g., Pb^{2+}, Eu^{2+}, Sn^{2+}, Cu^{2+}) at the B site, and halide anions (I^-, Br^-, Cl^-) at the X site.

Perovskite emitters show size-insensitively very narrow spectra (FWHM ~20 nm) in wide wavelength range (400 nm ≤ λ ≤ 780 nm) according to their inherent crystal structure (Fig. 2*B*). Therefore, they can have a very wide color gamut in Commission Internationale de l'Éclairage diagram. This highlights that perovskites can be promising emitters especially in display fields. On the other hand, organic emitters showed broad spectra (FWHM ≥40 nm) in large dimension (≥10 nm) and inorganic QD emitters showed relatively narrow (FWHM ~30 nm) but size-sensitive spectra in limited dimension (≤10 nm) (Fig. 2*C*).

The polar lead–halide bonds in perovskite crystal induce the Fröhlich interaction between charge carriers and longitudinal optical (LO) phonons, which results in LO phonon scattering and electron–phonon coupling; these predominantly determine the linewidth of emission spectrum (FWHM ~20 nm) (44). Furthermore, the traps and impurities in perovskites, which can arise from the low crystallinity, do not make a significant effect on the FWHM because trap-assisted recombination is mostly nonradiative decay and impurity-contributed linewidth broadening is negligible, respectively (44, 45). Thus, perovskites showed the size-insensitive FWHM, which is only affected by the crystal structure rather than quality and dimension of perovskite crystal.

In general, photoexcitation or charge carrier injection by external field forms geminate electron–hole pairs, which can (*i*) be dissociated into free charge carriers or (*ii*) form excitons (46, 47). The E_b reflecting the strength with which geminate electron–hole pairs are bound and the excitation density affecting the frequency with which

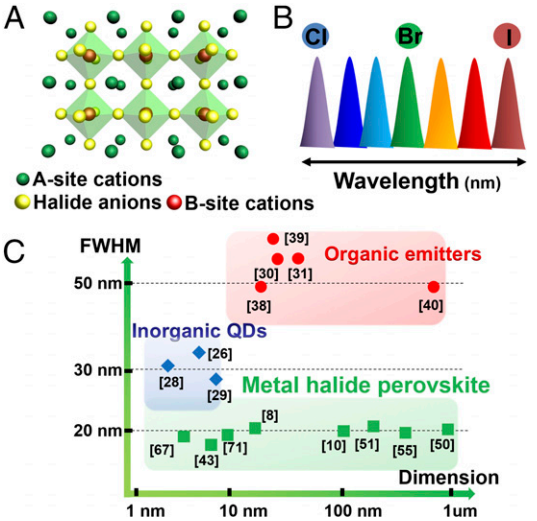

Fig. 2. (*A*) Schematic of crystal structure, (*B*) schematic of emission of metal halide perovskites, and (*C*) FWHM and dimension of perovskite, inorganic QD, and organic emitters.

electrons and holes meet together determine the ratio of free carriers and excitons ($n_{fc}/n_{e\text{-}h}$, where n_{fc} is the number of free carriers and $n_{e\text{-}h}$ is the number of geminate electron–hole pairs) (46). Many researchers have claimed that perovskites have Wannier-type excitons with low E_b (e.g., 76 or 150 meV for $CH_3NH_3PbBr_3$) and high dielectric constant (46–48). Thus, at RT, most of Wannier excitons dissociate into free carriers ($n_{fc}/n_{e\text{-}h} \sim 1$) because there is almost no electron–hole wavefunction overlap and exciton–exciton interaction (46). Charge trapping by trap states also induces the dissociation of excitons into free carriers and the nonradiative recombination pathways of free carriers and excitons, and thereby limits the luminescence efficiency at low fluences (47).

However, high excitation density of $>10^{20}$ cm^{-3} increases the number of charge carriers and wavefunction overlap of them in perovskites, fills the trap states, and thus leads to favorable exciton formation over dissociation into free carriers ($n_{fc}/n_{e\text{-}h} << 1$) (46, 47). Decreasing temperature <190 K induces less trap states and thus increases the proportion of excitons (46, 47). Confining perovskite crystal size to <10 nm can also increase the electron–hole wavefunction overlap and form the excitons rather than free carriers; colloidal PeNPs with small size of <10 nm showed the large electron–hole wavefunction overlap, excitonic behavior, and thereby much improved PLQE even at RT and low excitation fluences (43). These methods, which increase the electron–hole wavefunction overlap and fill the trap states, can improve the radiative recombination and increase PLQE up to ~95% (46, 47).

Renaissance of Perovskite Emitters: Bulk Polycrystalline Film Technology

Bright PeLEDs (>100 $cd \cdot m^{-2}$) based on PePCs at RT were first reported by Friend and coworkers (8) in 2014. They fabricated visible-light–emitting PeLEDs (>100 $cd \cdot m^{-2}$) using methylammonium (MA, $CH_3NH_3^+$)-based perovskites ($MAPbBr_3$) (EQE_{max} = 0.1% and maximum luminance L_{max} = 364 $cd \cdot m^{-2}$) and infrared-light–emitting PeLEDs using $MAPbI_3$ (EQE_{max} = 0.76% and maximum radiance R_{max} = 13.2 $W \cdot sr^{-1} \cdot m^{-2}$). At the almost same time, Lee and coworkers also fabricated bright visible PeLEDs (EQE_{max} = 0.125% and L_{max} = 417 $cd \cdot m^{-2}$) by using modified interlayers (9). These works demonstrated that pure perovskites can emit bright EL with very high color purity at RT. Many subsequent studies used a variety of experimental approaches to improve the luminescence efficiencies of PeLEDs (8–10, 49–66).

In 2015, Lee and coworkers first showed the possibility of high-efficiency PeLEDs (EQE_{max} = 8.53%) comparable to those of OLEDs (10) (Fig. 3*A* and Table 1). These increases in EQE of PeLEDs resemble the dramatic increase in power conversion efficiency of perovskite solar cells and demonstrate the great potential of perovskite emitters. To increase the efficiency of PeLEDs, the origins of low device efficiency were identified and many solutions were developed or suggested (8–10, 49–66). We categorize these approaches into (*i*) use of interlayers and (*ii*) modification of perovskite layers.

Use of Interlayers to Improve Device Efficiency. Conventional PeLEDs consist of anode, hole transport layer (HTL), perovskite emission layer (EML), electron transport layer (ETL), and cathode (Fig. 3*B*). One useful method to increase device efficiency is to use a variety of interlayers (Fig. 3*C*). PeLEDs without interlayers showed the severe exciton quenching, large charge injection barrier, nonuniform perovskite film coverage, and thus very low EL efficiencies (9, 52, 61). Use of appropriate interlayers between electrodes and perovskite EMLs can facilitate charge injection by reducing injection barriers (9, 49, 52, 55, 61). Furthermore, interlayers with modified surface energy or surface groups can contribute to the formation of uniform perovskite layers, reduce the leakage current, and improve the luminescence efficiencies of PeLEDs (10, 55, 61).

Lee and coworkers (9) used perfluorinated ionomers (PFI) with poly(3,4-ethylenedioxythiophene):poly(styrenesulfonate) (PEDOT:PSS) to reduce the hole injection barrier and exciton quenching at the PEDOT:PSS/PePC interface. Mixing a PFI with PEDOT:PSS resulted in the self-organization of PEDOT:PSS and PFI during spin-coating; the result was a gradient depth profile of PFI and gradient increase of work function from 5.2 eV (bottom)

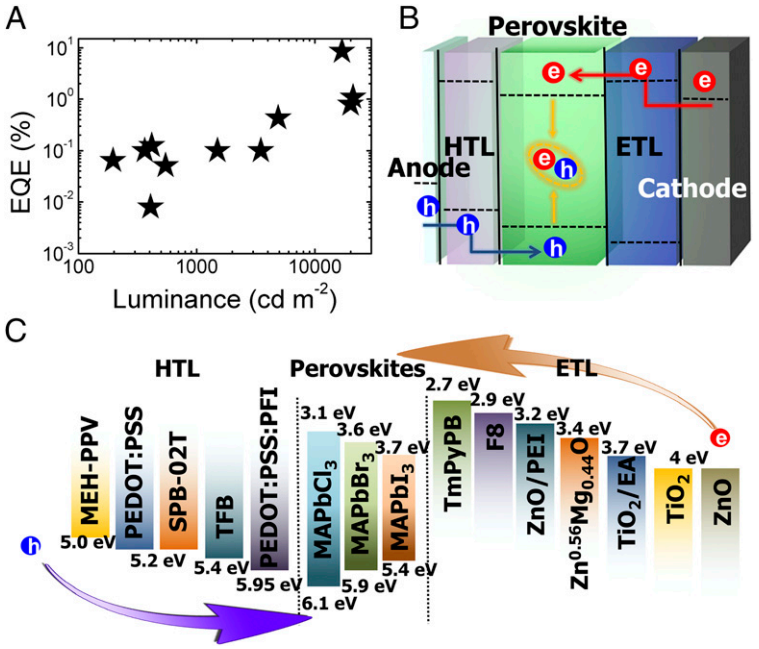

Fig. 3. (*A*) External quantum efficiency versus luminance characteristics of visible PeLEDs. Data are taken from refs. 8–10 and 49–64. (*B*) Schematic of PeLED structure and operation and (*C*) energy level diagram of materials used for HTL, ETL, and perovskite.

Table 1. Overview of reported results from PePC-based LEDs

Previous reports (ref.)	Publication year/month	Emission layer	FWHM, nm	CE_{max}, cd·A^{-1}	R_{max}, W·sr^{-1}·m^{-2}	EQE_{max}, %	L_{max}, cd·m^{-2}
Tan et al. (8)	2014/08	$MAPbBr_3$	20 (green)	0.3	13.2	0.1 (green) 0.76 (IR)	364
		$MAPbI_3$	35 (IR)				
Kim et al. (9)	2014/11	$MAPbBr_3$	~20	0.577	n.r.	0.125	417
Hoye et al. (49)	2015/01	$MAPbBr_3$	25	~0.27	n.r.	n.r.	550
Kumawat et al. (50)	2015/01	$MAPbBr_3$ (green)	30.9 (green)	~1.8×10^{-2} (green)	5×10^{-3}	~6.5×10^{-3} (green)	20 (green)
		$MAPbI_{1.19}Br_{1.37}Cl_{0.44}$ (red)	40.6 (red)	~2.8×10^{-4} (red)		0.28 (red)	0.26 (red)
		$MAPbI_{3-x}Cl_3$ (IR)	32.7 (IR)			0.18 (IR)	
Li et al. (51)	2015/02	$MAPbBr_3$	19	n.r.	n.r.	1.2	~2,500
Wang et al. (52)	2015/02	$MAPbBr_3$	22 (green)	n.r.	28	~0.8 (green)	~20,000
		$MAPbI_{3-x}Cl_x$	37 (IR)			3.5 (IR)	
Sadhanala et al. (53)	2015/02	$MAPbI_{3-x}Cl_x$	~41	n.r.	n.r.	0.024	—
Qin et al. (54)	2015/03	$MAPbBr_3$	20	n.r.	n.r.	~0.1	~1,500
Yu et al. (55)	2015/05	$MAPbBr_3$	41	0.22	n.r.	0.051	~545
Kumawat et al. (56)	2015/06	$MAPbBr_{1.86}Cl_{1.14}$ (green)	~40 (green)	~9×10^{-3} (green)	n.r.	~3×10^{-4} (blue)	~1.2 (green)
		$MAPbBr_{1.08}Cl_{1.92}$ (blue)	~20 (blue)	~3.5×10^{-4} (blue)			
Yantara et al. (57)	2015/10	$CsPbBr_3$	18	0.035	n.r.	0.008	407
Yu et al. (58)	2015/11	$MAPbBr_3$	~20	0.43	n.r.	0.1	3,490
Cho et al. (10)	2015/12	$MAPbBr_3$	~20	42.9	n.r.	8.53	16,936
Bade et al. (59)	2015/12	$MAPbBr_3$	~20	4.91	n.r.	1.1	21,014
Bi et al. (63)	2016/01	FAPbI3	n.r.	n.r.	n.r.	~0.5	n.r.
Shi et al. (60)	2016/03	$MAPbBr_3$	30	0.12	n.r.	0.0645	196
Wang et al. (61)	2016/04	$MAPbBr_3$	~25	n.r.	n.r.	0.43	4,890
Byun et al. (65)	2016/06	$(C_6H_5C_2H_4NH_3)_2MA_{m-1}Pb_mBr_{3m+1}$	~20	4.9	n.r.	n.r.	2935
Yuan et al. (66)	2016/06	$(C_6H_5C_2H_4NH_3)_2MA_{n-1}Pb_nBr_{3n+1}$	~50	n.r.	80	8.8	n.r.

m, 1–4, integer; n, integer; n.r., not reported.

to 5.95 eV (surface) (9). The rich PFI on the surface effectively blocked exciton quenching at the interface between PEDOT:PSS: PFI and $MAPbBr_3$ (9). With these strategies, the current efficiency *CE* of PeLEDs increased from 1.65×10^{-3} to 0.577 cd·A^{-1}, and the luminance improved from 1.38 to 417 cd·m^{-2} (9).

Also, electron injection barriers from cathodes to perovskite layers must be overcome in inverted structure PeLEDs. Hoye et al. (49) used spatial atmospheric atomic layer-deposited (SAALD) ZnO layers as electron transport layers instead of previously reported polyfluorene (8). The PeLEDs based on SAALD ZnO exhibited a very low turn-on voltage $V_{turn\text{-}on} = 2$ V, and $L_{max} = 550$ cd·m^{-2}. Polyethyleneimine (PEI) interlayers decreased the electron affinity of ZnO layers from 3.7 to 3.2 eV, and thereby made ohmic electron injection into perovskite layers possible (52). Furthermore, the hydrophilic surface of PEI-treated ZnO layers improved the uniformity of perovskite layers. With these modifications, $MAPbBr_3$ PeLEDs exhibited very high L_{max} of ~20,000 cd·m^{-2} and EQE_{max} of 0.8%, and $MAPbI_{3-x}Cl_x$ infrared PeLEDs exhibited R_{max} of ~28 W sr^{-1}·m^{-2} and EQE_{max} of 3.5%, respectively (52). These dramatically increased EQE_{max} compared with previous works (8, 9, 49, 50) are possibly due to the well-optimized film morphology of perovskite layers and reduced charge injection barriers.

Modification of Perovskite Layers. Uniform morphology of perovskite layers can also be achieved by modifying the process by which perovskite layers are formed. Spontaneous crystallization of perovskites by spin-coating often causes nonuniform and discontinuous film with scattered perovskite crystals (10). An effective method to overcome this nonuniformity is to use nonpolar solvent dripping (10, 67). By dripping nonpolar solvents (e.g., chloroform, chlorobenzene, toluene) that do not dissolve perovskite precursors onto the wet perovskite films during spin-coating, aprotic polar solvents [e.g., dimethylformamide (DMF), dimethyl sulfoxide (DMSO), and γ-butyrolactone] can be washed away and immediate crystallization of perovskites occurs; the result is a uniform and dense film (10). In perovskite solar cells, the solvent dripping was designed not for rapid pinning of crystal growth to achieve small grains but for making uniform PePCs with large grain size to facilitate the diffusion and dissociation of excitons; however, the process cannot be applied to PeLEDs because the grain size should be decreased to increase the luminescence efficiencies of PePCs (10). Decreased grain size and increased area of grain boundary can spatially confine excitons or charge carriers and block their diffusion, and, as a consequence, increase the radiative recombination. Therefore, it is necessary to develop an optimal solvent-dripping process that can fabricate PePCs with minimal grain size. Use of DMSO (which has a higher boiling point of 189 °C than DMF, which has boiling point of 153 °C) as a solvent can delay spontaneous crystallization of perovskites and thereby facilitate the optimization of solvent-dripping process (10). Also, the perovskite's crystallization behavior and the final film morphology depend on the physical properties of dripping solvents (68). Therefore, the choice of dripping solvents to fabricate perovskite films most suitable for PeLEDs is an important task. Dripping of chloroform, a highly volatile solvent (boiling point, 61.2 °C), on the growing quasifilm during spin-coating of $MAPbBr_3$/DMSO with the optimized dripping conditions resulted in small $MAPbBr_3$ grains (100–250 nm) possibly because of minimized crystal growth time after supersaturation (10). This process was called as "nanocrystal pinning" (NCP).

The NCP by a volatile polar solvent (S-NCP) was modified to further decrease the grain size. Additive-based NCP (A-NCP), in which organic small molecules 2,2′,2″-(1,3,5-benzinetriyl)-tris(1-phenyl-1-*H*-benzimidazole) (TPBI) were included in the dripping solvent (chloroform), effectively inhibited growth of $MAPbBr_3$ crystals and substantially reduced $MAPbBr_3$ average grain size to 99.7 nm. PeLEDs based on A-NCP exhibited significantly high EQE_{max} of 8.53% and maximum *CE* of 42.9 cd·A^{-1} (10).

Another method to create uniform film morphology is to control the solubility of perovskite precursors and crystallization rate of perovskites (58). HBr incorporation into $MAPbBr_3$/DMF

solutions increased the solubility of $MAPbBr_3$ and decreased the crystallization rate; the HBr concomitantly increased supersaturation concentration and reduced the final film thickness; uniform and continuous $MAPbBr_3$ films resulted (58). Using this approach with optimized HBr concentration (6 vol%), bright PeLEDs with EQE_{max} of 0.1% and L_{max} of 3,490 $cd{\cdot}m^{-2}$ were achieved (58).

To fill the voids in perovskite crystals, an insulating polymer, polyimide precursor (PIP), was mixed in perovskite solutions (51). The presence of PIP between the scattered $MAPbBr_3$ crystals blocked the flow of leakage current, which caused significant reduction in EL efficiency. The composite film was optimized at the ratio of $MAPbBr_3$:PIP = 1:1 (wt/wt), and the corresponding PeLEDs showed EQE_{max} of 1.2% (51).

Although a uniform morphology can be achieved by using various strategies described above, the luminescent property of perovskite films can be further improved by controlling the precursor ratio (10, 57). The use of MABr-rich $MAPbBr_3$ solutions resulted in significantly enhanced EQE and luminance, because slightly excess MABr made well-matching stoichiometry and prevented the formation of metallic Pb atoms that strongly quench luminescence (10). The precursor ratio, MABr:$PbBr_2$, was optimized at 1.05:1 (mol:mol) because the insulating nature of more excess MABr can block efficient charge transport. Using the optimized precursor ratio of MABr:$PbBr_2$ of 1.05:1, >100 times higher *CE* (21.4 $cd{\cdot}A^{-1}$) was obtained than that of the device with equimolar precursor ratio (0.183 $cd{\cdot}A^{-1}$) (10). The control of precursor ratio is also useful in the all-inorganic perovskite $CsPbBr_3$ (57).

The use of quasi-2D perovskite structures can also be a useful strategy to increase the efficiency of PeLEDs (65, 66). Very recently, high-efficiency quasi-2D PeLEDs based on MA-phenylethyl ammonium (PEA) mixed cations were reported (65, 66). The optimized MA:PEA ratio led to the improved uniformity of perovskite film, strong exciton confinement, and the decrease in trap density, resulting in high-efficiency green PeLEDs (CE_{max} = 4.90 $cd{\cdot}A^{-1}$) (65). The highly efficient infrared PeLEDs (EQE_{max} = 8.8%) based on the quasi-2D perovskite structure ($PEA_2(MA)_{n-1}Pb_nI_{3n+1}$) were shown with the systematic investigation on the charge carrier funneling (66).

Next-Generation Emitters: Perovskite Nanoparticle Technology

Although luminescence efficiencies of PeLED based on PePCs have increased, their large size grains (≥100 nm) still provide the dissociation of excitons into free carriers and nonradiative recombination. PePC films and PePC–PeLEDs also showed low PL and EL efficiencies at low excitation density ($<10^{20}$ cm^{-3}) and applied bias, respectively, because of little electron–hole wavefunction overlap and a lot of unfilled trap states under low excitation density and applied bias. Therefore, to further improve the EL efficiencies in PeLEDs, luminescence efficiencies at low applied bias need to be improved (8, 10). In this sense, PeNPs with small crystal size (<10 nm) that can emit maximum PL and EL efficiencies at low excitation density or applied bias can be a promising alternative strategy (69–72).

The increased exciton confinement and exciton binding energy in a small volume of PeNPs can increase the radiative recombination caused by exciton recombination rather than by free carrier recombination (43, 69–74). Furthermore, PeNPs showed much less subband defect states than did PePCs due to small size, when their surface defects were chemically well passivated (71, 72). Thus, PeNPs, well passivated by chemical ligands, can show high PLQE at low electric field or excitation density (71, 72).

The first PeNPs were fabricated using the hard-template approach by depositing perovskite precursor solution into Al_2O_3 nanoporous film (42). Although these nanocrystals showed size controllability and did not use a surfactant ligand, they could not be used in LEDs because they need a nanoporous hard template such as Al_2O_3 or TiO_2 (42, 75). For application to LEDs and other optoelectronics, colloidal NPs synthesized by solution reaction were demonstrated. The first colloidal PeNPs were synthesized by "nontemplate" (NT) methods, which can synthesize monodispersed PeNPs in solution (69). The authors formed colloidal PeNPs by adding MA bromide (MABr) and $PbBr_2$ into a mixture of oleic acid, octadecene, and long-chain alkyl ammonium bromide as a ligand, at 80 °C. The first PeNPs synthesized by NT methods showed PLQE of 20% and good dispersability in various protic solvents (69). PLQE was increased to 83% by finely tuning the molar ratio of MABr, $PbBr_2$, and ligands (70).

Recently, Kovalenko and coworkers (43) reported all-inorganic metal halide PeNPs, $CsPbX_3$ (X = Cl, Br, I) that showed PLQE of >90%, high color purity ($12 \leq FWHM \leq 42$ nm), wide color tunability of 410–700 nm, and wide color gamut of 140% of the National Television System Committee color standard. The PeNPs were synthesized using the "hot-injection" (HI) method, in which the Cs-oleate is injected into a mixture of oleic acid, oleylamine, and PbX_2 in octadecene solution at a temperature of >140 °C. The emission color and size can be controlled by adjusting reaction time and temperature (43, 76, 77). This method imitates the synthesis route of colloidal chalcogenide QDs such as CdSe QDs, but is much simpler than those of colloidal inorganic QDs because PeNPs do not need complex surface passivation process (20–29). However, HI methods still use toxic and unstable organic solvents, and must be conducted in a nitrogen environment at high temperature (>140 °C), so the prospects of commercialization may be limited (43, 76–78).

Recently, Zhang et al. (71) reported $MAPbBr_3$-based PeNPs synthesized at RT, which had PLQE of >70%, good color purity, and color tunability. All-inorganic PeNPs ($CsPbX_3$) can also be synthesized by the same process with $MAPbBr_3$ PeNPs synthesized at RT (78). The authors synthesized colloidal NPs by dropping a perovskite precursor solution in a good solvent (e.g., DMF) to a bad solvent (e.g., toluene) under vigorous stirring. Due to poor solubility of perovskites in a bad solvent, they recrystallized when they met the supersaturated state; they were stabilized using two different ligands (e.g., oleic acid and oleylamine) (71, 78). These PeNPs synthesized at RT showed similar high PLQE, color purity, and stability with those synthesized by HI methods, but did not require inert environmental and hot temperature, and thus are compatible with industrial mass production due to high yield at low cost (71, 78).

The first ELs from PeNPs were reported by Pérez-Prieto and coworkers (69) in 2014. In April 2015, Costa and coworkers (79) increased L_{max} of PeNP-based light-emitting electrochemical cells to 1.3 cd/m^2 by embedding PeNPs in the electrolyte matrix (mixture of $LiCF_3SO_3$ and trimethylolpropane ethoxylate). Then, Zeng and coworkers (77) first developed red–green–blue (RGB)-emitting all-inorganic PeNP-LEDs. After those pioneering researches, EQE_{max} and L_{max} of PeNP-LEDs have dramatically increased to 5.7% and 206 cd/m^2 for red-emitting devices, and to 0.48% and 10,590 cd/m^2 for green-emitting devices in only 2 y, respectively (77, 79–82) (Table 2). These increases in luminescence efficiencies of PeNP-LEDs are much faster than the improvement of EQE_{max} in LEDs based on inorganic QDs (Fig. 4*A*). Subsequently, many groups have developed high-efficiency PeNP-LEDs by using (*i*) interlayer control and (*ii*) PeNP film modification (80–82).

Rogach and coworkers (80) improved the EL efficiency of PeNP-LEDs by interlayer control. They reduced the hole injection barrier from 1.09 to 0.75 eV by applying thin PFI layer (~5 nm) on top of poly(*N*,*N*′-bis(4-butylphenyl)-*N*,*N*′-bis(phenyl)-benzidine) (poly-TPD). Furthermore, PFI prevented the charge transfer between poly-TPD and perovskite layers and luminescence quenching. As a consequence of improved hole injection and prevented luminescence

Table 2. Summary of published results from PeNP-based LEDs and inorganic QD-based LEDs

Previous reports (ref.)	Publication year/month	Emission layer	FWHM, nm	CE_{max}, cd·A^{-1}	PE_{max}, lm·W^{-1}	EQE_{max}, %	L_{max}, cd·m^{-2}
Schmidt et al. (69)	2014/01	$MAPbBr_3$	22	n.r.	n.r.	n.r.	~0.5
Aygüler et al. (79)	2015/04	$MAPbBr_3$	~200 ($MAPbBr_3$)	0.013 ($MAPbBr_3$)	n.r.	n.r.	1.8 ($MAPbBr_3$)
		$FAPbBr_3$	~200 ($FAPbBr_3$)	0.005 ($FAPbBr_3$)			0.8 ($FAPbBr_3$)
Song et al. (77)	2015/10	$CsPbCl_{3-x}Br_x$	<30	0.14 (blue)	0.07 (blue)	0.07 (blue)	742 (blue)
		$CsPbBr_3$		0.43 (green)	0.18 (green)	0.12 (green)	946 (green)
		$CsPbI_{3-x}Br_x$		0.08 (orange)	0.06 (orange)	0.09 (orange)	528 (orange)
Zhang et al. (80)	2016/01	$CsPbBr_3$	18	0.19	n.r.	0.06	1,377
Ling et al. (81)	2015/11	$MAPbBr_3$	20	n.r.	1	0.48	10,590
Li et al. (82)	2016/03	$CsPbCl_{1.5}Br_{1.5}$	17 (blue)	n.r.	n.r.	0.0074 (blue)	8.7 (blue)
		$CsPbBr_3$	19 (green)			0.19 (green)	2,335 (green)
		$CsPbI_{2.25}Br_{0.75}$	29 (orange)			1.4 (orange)	1,559 (orange)
		$CsPbI_3$	31 (red)			5.7 (red)	206 (red)
Mattoussi et al. (21)	1998/06	CdSe	~30	n.r.	n.r.	0.1	n.r.
Schlamp et al. (22)	1997/08	CdSe/CdS	~50	n.r.	n.r.	0.22	600
Coe et al. (23)	2002/12	CdSe/ZnS	32	1.6	n.r.	0.52	2,000
Coe-Sullivan et al. (24)	2005/04	PbSe	27	n.r.	>1	>2	>7,000
Cho et al. (25)	2009/05	CdSe/CdS/ZnS	35	2.53	2.41	n.r.	12,380
Kwak et al. (26)	2012/04	Cd1−xZnxS@ZnS	~20	0.4 (blue)	n.r.	1.7 (red)	2,250 (blue)
		CdSe@ZnS	~30	19.2 (green)		5.8 (green)	218,800 (green)
		CdSe/CdS/ZnS	~30	5.7 (red)		7.3 (red)	23,040 (red)
Qian et al. (27)	2011/08	CdSe/ZnS	28	0.32 (blue)	0.17 (blue)	0.22 (blue)	4,200 (blue)
			38	7.5 (green)	8.2 (green)	1.8 (green)	68,000 (green)
			39	3.9 (red)	3.8 (red)	1.7 (red)	31,000 (red)
Mashford et al. (28)	2013/04	CdSe/CdS	~25	19	25	18	>50,000
Dai et al. (29)	2014/12	CdSe/CdS	28	n.r.	n.r.	20.5	42,000

n.r., not reported.

quenching, PeNP-LEDs showed the improved *CE* from 0.08 to 0.19 cd·A^{-1} and EQE_{max} from 0.026% to 0.06%, respectively (80).

Gao and coworkers (81) improved the luminescence efficiencies of PeNP-LEDs by coating poly(9-vinylcarbazole):2-(4-biphenylyl)-5-phenyl-1,3,4-oxadiazole (PVK:PBD) layers on PeNP layers. PVK:PBD cohost layer improved the charge balance in devices and reduced the film roughness by covering voids and holes in PeNP films (Fig. 4*B*). PeNP-LEDs with PVK:PBD layers exhibited much improved L_{max} of 10,590 cd·m^{-2} and EQE_{max} of 0.48% compared with those without PVK:PBD layers (L_{max} of 1,113 cd·m^{-2} and EQE_{max} of

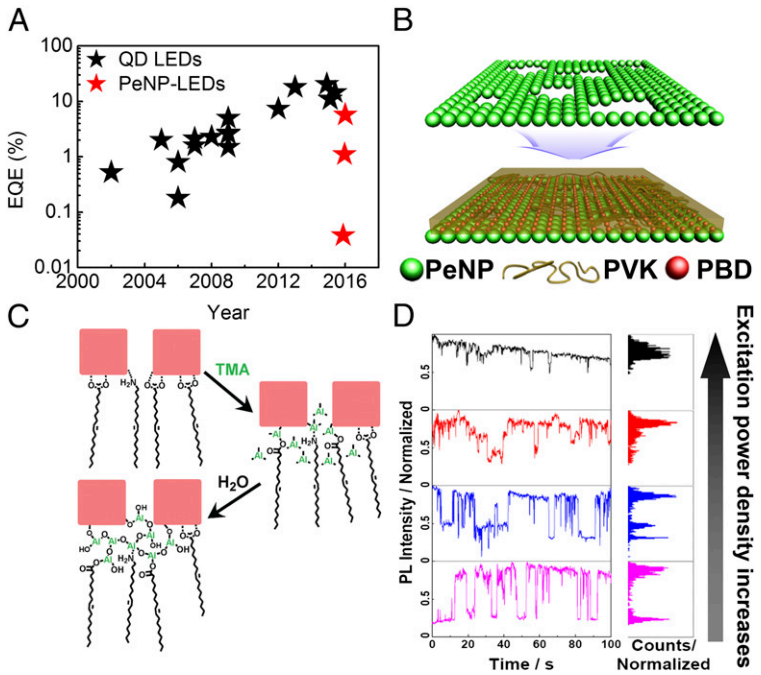

Fig. 4. (*A*) External quantum efficiency characteristics of QD LEDs and PeNP-LEDs. Data are taken from references as follows: QD LEDs, refs. 20–29; PeNP-LEDs, refs. 79–82. (*B*) Schematic of $MAPbBr_3$ PeNP/PVK:PBD layer as reported in ref. 81 (inspired by a similar drawing in ref. 81). (*C*) Schematic of cross-linking process. Reproduced from ref. 82 with permission from Wiley-VCH. (*D*) PL transients measured at different excitation power density. Reproduced from ref. 83 with permission from American Chemical Society.

0.038%). Recently, Tan and coworkers (82) dramatically improved the EQE_{max} of PeNP-LEDs by using vapor cross-linking methods. They created a hydroxide-terminated aluminum oxide network between PeNPs by exposing them to trimethylaluminum (TMA) vapor (Fig. 4*C*). This cross-linking method can increase the PL intensity by increasing the crystal spacing and passivating the surface defects of NPs. With this cross-linking method, PeNP-LEDs achieved remarkably high $EQE_{max} = 5.7\%$, which is 10 times higher than that of non–cross-linked devices (82). Furthermore, this cross-linking method can be applied to various RGB-emitting PeNP films and demonstrate multicolor emitting PeNP-LEDs.

Although PeNPs showed excitonic behavior due to much improved wavefunction overlap, high E_b, and high PLQE at RT and low excitation fluences, and PeNP-LEDs showed the dramatically increasing luminescence efficiencies, large number of surface defects arising from high surface-to-volume ratio (S/V) should be passivated for higher efficiency and stability. PeNPs have much more defects and trap density [$(1.9–7.6) \times 10^{18}$ cm^{-3} for 10-nm $MAPbBr_3$ particles] than do millimeter-sized $MAPbBr_3$ large crystals (5.7×10^9 cm^{-3}) or $MAPbI_3$ thin-film polycrystals (~10^{16} cm^{-3}) due to high S/V when their surface defects are not chemically passivated (73, 83). These surface defects can induce nonradiative decay of excitons in grain boundaries and consequently induce smaller PL intensity and high amplitude of PL blinking (10^7 photons $cd^2 \cdot W^{-1} \cdot s^{-1}$) (73, 74, 83). These severe PL blinking and numerous surface defects in PeNPs can be prevented by irradiation with light, reaction with Lewis bases, and self-passivation of Pb–halogen composites (e.g., $PbBr_x$) (73, 78, 83, 84).

Considering the explosive improvement of EQE_{max} in PeNP-LEDs and various surface trap-passivating methods, we anticipate that the luminescence efficiencies of PeNP-LEDs will catch up with those of inorganic QD LEDs or OLEDs in the near future.

Future Directions

The huge impact of perovskite emitters is manifested by its explosive increase in luminescence efficiencies and fundamental research including dynamics of charge carriers (e.g., excitons, multiexcitons, and free carriers) (85) and quantum confinement effects (86). Their low material costs also provide a high possibility of their wide application in industry. However, there are still many technological and scientific challenges: the 8.53% of EQE_{max} in PeLEDs remains below that of QD LEDs (~20%) and OLEDs (~30%). We expect the EQE of PeLEDs will eventually increase up to 25~30% envisaging the future improvement in the PLQE of perovskite emitters up to 100%, the charge balance factor of PeLEDs up to 100%, and the common level of outcoupling efficiency of 25~30% (87). Furthermore, few studies on device stability and environmentally benign perovskite emitters have been conducted. Here, we suggest future research directions of perovskite emitters that can attract many researcher's attention.

To further increase the EL efficiencies of PeLEDs, reducing the grain size of PePCs down to exciton Bohr diameter D_B can be effective. The D_B of $MAPbBr_3$ can be calculated according to the following equation:

$$r_B = \frac{\varepsilon_r m_0}{\mu} 0.053 \approx 5 \text{ nm},$$

where r_B is the exciton Bohr radius, $\varepsilon_r \sim 16$ is the dielectric constant, and $\mu \sim 0.12 m_0$ is the reduced mass of $MAPbBr_3$ (88, 89). Thus, decreasing the grain size to ~10 nm (near D_B) by adding crystal-pinning agents can maximize the EQE_{max} considering trade-off between large surface traps that can act as nonradiative recombination sites in grains $< D_B$ (73, 74), and thermal ionization of charge carriers in grains $> D_B$. Especially, different fabrication methods such as coevaporation of perovskite precursors and organic semiconductors may offer a new possibility of efficient energy transfer system in host–guest (organic–perovskite) EML. The guest–host (QD–perovskite) system (90, 91) can also show the potential of perovskite in different applications.

The relatively higher refractive index *RI* of perovskites ($\eta_{perov} > 2.0$) compared with those of organic films ($\eta_{organic} \sim 1.7$) and glass substrate ($\eta_{glass} \sim 1.5$) can induce the internal reflection at the ETL/perovskite or HTL/perovskite interfaces and severe light trapping (i.e., optical loss), and thus reduce the EL efficiency (87, 92, 93). Therefore, various light extraction techniques such as use of *RI*-matching substrate or additional layer, optimization of LED structures, light-extracting structures (e.g., microlens arrays, etching the glass substrate, nanostructures, photonic crystals), and surface plasmons can further enhance the EL efficiencies of PeLEDs (87, 94).

To improve the stability of perovskite emitters, substituting Cs cations or FA cations to MA cations can be effective (11, 12). $FAPbBr_3$ is a promising candidate for EML in green light-emitting PeLEDs with high photo, moisture, and thermal stability. Although FA-based perovskites offer high stability, their charge carrier mobilities are much inferior to MA-based perovskites, which limits luminescence efficiencies and brightness in PeLEDs; therefore, to complement the inferior charge carrier mobilities, research on finding an optimal film morphology and device structure is required. $CsPbBr_3$ showed much higher onset temperature of evaporation/deposition (~580 °C) than did $MAPbBr_3$ (~220 °C) (12); thus, Cs-based perovskites can be an important research topic for achieving high stability in PeLEDs. Introduction of a quasi-2D perovskite structure (13, 14) and a fluorinated ammonium cations (15), cross-linking of perovskite crystals (16), and Lewis base treatment of perovskite layers (73) can be also effective ways to improve device stability.

Furthermore, a toxicity problem of perovskite due to center Pb metal should be solved. Pb-free perovskite emitters were reported; however, the PLQE was very low (<0.14%) and EL has not been reported yet, possibly due to the severe instability, and defects or trap states by emergence of Sn^{4+} center (17–19). Some approaches, such as reducing hole-doping density and using stabilizers that reduce Sn vacancies and traps, may improve the stability of Pb-free perovskite EML and environmentally benign PeLEDs (17–19). With these approaches, perovskite emitters can be investigated for use in other applications such as bioimaging as well as displays and solid-state lightings.

Research on the few atomic levels of perovskites may also offer a fundamental understanding of complex properties in quantum size regime. Atomically very thin 2D perovskite showed the structural relaxation, enhanced PL intensity, and increased band gap compared to the bulk perovskite (95, 96). Further research on charge dynamics, quantum effects, and structural mechanics may create a new range of applications.

Despite the remaining challenges of perovskite emitters in terms of limited efficiency, instability, and toxicity, the high color purity and low material costs of perovskite emitters are very attractive for industrial applications (especially for displays). We envisage that these advantages and potentials of perovskite emitters will encourage researchers to collaborate to solve the remaining challenges and to make a synergetic effect in multidisciplinary fields such as physics, chemistry, and engineering.

Acknowledgments

This work was supported by the National Research Foundation of Korea (NRF) Grant funded by the Korean government (Ministry of Science, ICT & Future Planning) (NRF-2016R1A3B1908431).

1 Era M, Morimoto S, Tsutsui T, Saito S (1994) Organic-inorganic heterostructure electroluminescent device using a layered perovskite semiconductor $(C_6H_5C_2H_4NH_3)_2PbI_4$. *Appl Phys Lett* 65(6):676–678.
2 Hong X, Ishihara T, Nurmikko AV (1992) Photoconductivity and electroluminescence in lead iodide based natural quantum well structures. *Solid State Commun* 84(6):657–661.
3 Hattori T, Taira T, Era M, Tsutsui T, Saito S (1996) Highly efficient electroluminescence from a heterostructure device combined with emissive layered-perovskite and an electron-transporting organic compound. *Chem Phys Lett* 254(1-2):103–108.
4 Ishihara T, Hong X, Ding J, Nurmikko AV (1992) Dielectric confinement effect for exciton and biexciton states in PbI_4-based two-dimensional semiconductor structures. *Surf Sci* 267(1-3):323–326.
5 Hong X, Ishihara T, Nurmikko AV (1992) Dielectric confinement effect on excitons in PbI_4-based layered semiconductors. *Phys Rev B* 45(12):6961–6964.
6 Ishihara T, Takahashi J, Goto T (1989) Exciton state in two-dimensional perovskite semiconductor $(C_{10}H_{21}NH_3)_2PbI_4$. *Solid State Commun* 69(9):933–936.
7 Chondroudis K, Mitzi DB (1999) Electroluminescence from an organic-inorganic perovskite incorporating a quaterthiophene dye within lead halide perovskite layers. *Chem Mater* 11(11):3028–3030.
8 Tan Z-K, et al. (2014) Bright light-emitting diodes based on organometal halide perovskite. *Nat Nanotechnol* 9(9):687–692.
9 Kim Y-H, et al. (2015) Multicolored organic/inorganic hybrid perovskite light-emitting diodes. *Adv Mater* 27(7):1248–1254.
10 Cho H, et al. (2015) Overcoming the electroluminescence efficiency limitations of perovskite light-emitting diodes. *Science* 350(6265):1222–1225.
11 Lee J-W, et al. (2015) Formamidinium and cesium hybridization for photo- and moisture-stable perovskite solar cell. *Adv Energy Mater* 5(20):1501310.
12 Kulbak M, et al. (2016) Cesium enhances long-term stability of lead bromide perovskite-based solar cells. *J Phys Chem Lett* 7(1):167–172.
13 Smith IC, Hoke ET, Solis-Ibarra D, McGehee MD, Karunadasa HI (2014) A layered hybrid perovskite solar-cell absorber with enhanced moisture stability. *Angew Chem Int Ed Engl* 53(42):11232–11235.
14 Cao DH, Stoumpos CC, Farha OK, Hupp JT, Kanatzidis MG (2015) 2D homologous perovskites as light-absorbing materials for solar cell applications. *J Am Chem Soc* 137(24):7843–7850.
15 Bi D, et al. (2016) High-performance perovskite solar cells with enhanced environmental stability based on amphiphile-modified $CH_3NH_3PbI_3$. *Adv Mater* 28(15): 2910–2915.
16 Li X, et al. (2015) Improved performance and stability of perovskite solar cells by crystal crosslinking with alkylphosphonic acid ω-ammonium chlorides. *Nat Chem* 7(9):703–711.
17 Jellicoe TC, et al. (2016) Synthesis and optical properties of lead-free cesium tin halide perovskite nanocrystals. *J Am Chem Soc* 138(9):2941–2944.
18 Noel NK, et al. (2014) Lead-free organic–inorganic tin halide perovskites for photovoltaic applications. *Energy Environ Sci* 7(9):3061–3068.
19 Lee SJ, et al. (2016) Fabrication of efficient formamidinium tin iodide perovskite solar cells through SnF_2–pyrazine complex. *J Am Chem Soc* 138(12):3974–3977.
20 Colvin VL, Schlamp MC, Allvisatos AP (1994) Light-emitting diodes made from cadmium selenide nanocrystals and a semiconducting polymer. *Nature* 370(6488): 354–357.
21 Mattoussi H, et al. (1998) Electroluminescence from heterostructures of poly(phenylene vinylene) and inorganic CdSe nanocrystals. *J Appl Phys* 83(12):7965–7974.
22 Schlamp MC, Peng X, Alivisatos AP (1997) Improved efficiencies in light emitting diodes made with CdSe(CdS) core/shell type nanocrystals and a semiconducting polymer. *J Appl Phys* 82(11):5837–5842.
23 Coe S, Woo W-K, Bawendi M, Bulović V (2002) Electroluminescence from single monolayers of nanocrystals in molecular organic devices. *Nature* 420(6917): 800–803.
24 Coe-Sullivan S, Steckel JS, Woo W-K, Bawendi MG, Bulovic̀ V (2005) Large-area ordered quantum-dot monolayers via phase separation during spin-coating. *Adv Funct Mater* 15(7):1117–1124.
25 Cho K-S, et al. (2009) High-performance crosslinked colloidal quantum-dot light-emitting diodes. *Nat Photonics* 3(6):341–345.
26 Kwak J, et al. (2012) Bright and efficient full-color colloidal quantum dot light-emitting diodes using an inverted device structure. *Nano Lett* 12(5):2362–2366.
27 Qian L, Zheng Y, Xue J, Holloway PH (2011) Stable and efficient quantum-dot light-emitting diodes based on solution-processed multilayer structures. *Nat Photonics* 5(9):543–548.
28 Mashford BS, et al. (2013) High-efficiency quantum-dot light-emitting devices with enhanced charge injection. *Nat Photonics* 7(5):407–412.
29 Dai X, et al. (2014) Solution-processed, high-performance light-emitting diodes based on quantum dots. *Nature* 515(7525):96–99.
30 Tang CW, VanSlyke SA, Chen CH (1989) Electroluminescence of doped organic thin films. *J Appl Phys* 65(9):3610–3616.
31 Adachi C, Baldo MA, Thompson ME, Forrest SR (2001) Nearly 100% internal phosphorescence efficiency in an organic light-emitting device. *J Appl Phys* 90(10): 5048–5051.
32 Chang Y-L, et al. (2012) Enhancing the efficiency of simplified red phosphorescent organic light emitting diodes by exciton harvesting. *Org Electron* 13(5): 925–931.
33 Kim DH, et al. (2011) Highly efficient red phosphorescent dopants in organic light-emitting devices. *Adv Mater* 23(24):2721–2726.
34 Baldo MA, et al. (1998) Highly efficient phosphorescent emission from organic electroluminescent devices. *Nature* 395(6698):151–154.
35 O'Brien DF, Baldo MA, Thompson ME, Forrest SR (1999) Improved energy transfer in electrophosphorescent devices. *Appl Phys Lett* 74(3):442–444.
36 Meerheim R, et al. (2008) Influence of charge balance and exciton distribution on efficiency and lifetime of phosphorescent organic light-emitting devices. *J Appl Phys* 104(1):014510.
37 Lee T-W, Chung Y, Kwon O, Park J-J (2007) Self-organized gradient hole injection to improve performance of polymer electroluminescent devices. *Adv Funct Mater* 17(3):390–396.
38 Han T-H, et al. (2012) Molecularly controlled interfacial layer strategy toward highly efficient simple-structured organic light-emitting diodes. *Adv Mater* 24(11): 1487–1493.
39 Kim Y-H, Wolf C, Cho H, Jeong S-H, Lee T-W (2016) Highly efficient, simplified, solution-processed thermally activated delayed-fluorescence organic light-emitting diodes. *Adv Mater* 28(4):734–741.
40 Kabra D, Lu LP, Song MH, Snaith HJ, Friend RH (2010) Efficient single-layer polymer light-emitting diodes. *Adv Mater* 22(29):3194–3198.
41 Uoyama H, Goushi K, Shizu K, Nomura H, Adachi C (2012) Highly efficient organic light-emitting diodes from delayed fluorescence. *Nature* 492(7428): 234–238.
42 Kojima A, Ikegami M, Teshima K, Miyasaka T (2012) Highly luminescent lead bromide perovskite nanoparticles synthesized with porous alumina media. *Chem Lett* 41(4):397–399.
43 Protesescu L, et al. (2015) Nanocrystals of cesium lead halide perovskites ($CsPbX_3$, X = Cl, Br, and I): Novel optoelectronic materials showing bright emission with wide color gamut. *Nano Lett* 15(6):3692–3696.
44 Wright AD, et al. (2016) Electron-phonon coupling in hybrid lead halide perovskites. *Nat Commun* 7(0):11755.
45 Wetzelaer G-JAH, et al. (2015) Trap-assisted non-radiative recombination in organic-inorganic perovskite solar cells. *Adv Mater* 27(11):1837–1841.
46 D'Innocenzo V, et al. (2014) Excitons versus free charges in organo-lead tri-halide perovskites. *Nat Commun* 5:3586.
47 Stranks SD, et al. (2014) Recombination kinetics in organic-inorganic perovskites: Excitons, free charge, and subgap states. *Phys Rev Appl* 2(3):034007.
48 Hu M, et al. (2015) Distinct exciton dissociation behavior of organolead trihalide perovskite and excitonic semiconductors studied in the same system. *Small* 11(18):2164–2169.

49 Hoye RLZ, et al. (2015) Enhanced performance in fluorene-free organometal halide perovskite light-emitting diodes using tunable, low electron affinity oxide electron injectors. *Adv Mater* 27(8):1414–1419.
50 Kumawat NK, Dey A, Narasimhan KL, Kabra D (2015) Near infrared to visible electroluminescent diodes based on organometallic halide perovskites: Structural and optical investigation. *ACS Photonics* 2(3):349–354.
51 Li G, et al. (2015) Efficient light-emitting diodes based on nanocrystalline perovskite in a dielectric polymer matrix. *Nano Lett* 15(4):2640–2644.
52 Wang J, et al. (2015) Interfacial control toward efficient and low-voltage perovskite light-emitting diodes. *Adv Mater* 27(14):2311–2316.
53 Sadhanala A, et al. (2015) Electroluminescence from organometallic lead halide perovskite-conjugated polymer diodes. *Adv Electron Mater* 1(3):1500008.
54 Qin X, Dong H, Hu W (2015) Green light-emitting diode from bromine based organic-inorganic halide perovskite. *Sci China Mater* 58(3):186–191.
55 Yu JC, et al. (2015) High-performance planar perovskite optoelectronic devices: A morphological and interfacial control by polar solvent treatment. *Adv Mater* 27(23):3492–3500.
56 Kumawat NK, et al. (2015) Band gap tuning of $CH_3NH_3Pb(Br_{1-x}Cl_x)_3$ hybrid perovskite for blue electroluminescence. *ACS Appl Mater Interfaces* 7(24): 13119–13124.
57 Yantara N, et al. (2015) Inorganic halide perovskites for efficient light-emitting diodes. *J Phys Chem Lett* 6(21):4360–4364.
58 Yu JC, Kim DB, Jung ED, Lee BR, Song MH (2016) High-performance perovskite light-emitting diodes via morphological control of perovskite films. *Nanoscale* 8(13):7036–7042.
59 Bade SGR, et al. (2016) Fully printed halide perovskite light-emitting diodes with silver nanowire electrodes. *ACS Nano* 10(2):1795–1801.
60 Shi Z-F, et al. (2016) High-performance planar green light-emitting diodes based on a PEDOT:PSS/$CH_3NH_3PbBr_3$/ZnO sandwich structure. *Nanoscale* 8(19): 10035–10042.
61 Wang N, et al. (2016) Morphology control of perovskite light-emitting diodes by using amino acid self-assembled monolayers. *Appl Phys Lett* 108(14):141102.
62 Sanchez RS, et al. (2016) Tunable light emission by exciplex state formation between hybrid halide perovskite and core/shell quantum dots: Implications in advanced LEDs and photovoltaics. *Sci Adv* 2(1):e1501104.
63 Bi D, et al. (2016) Efficient luminescent solar cells based on tailored mixed-cation perovskites. *Sci Adv* 2(1):e1501170.
64 Genco A, et al. (2016) Fully vapor-deposited heterostructured light-emitting diode based on organo-metal halide perovskite. *Adv Electron Mater* 2(3):1500325.
65 Byun J, et al. (2016) Efficient visible Quasi-2D perovskite light-emitting diodes. *Adv Mater* 28(34):7515–7520.
66 Yuan M, et al. (June 27, 2016) Perovskite energy funnels for efficient light-emitting diodes. *Nat Nanotechnol*, 10.1038/nnano.2016.110.
67 Jeon NJ, et al. (2014) Solvent engineering for high-performance inorganic-organic hybrid perovskite solar cells. *Nat Mater* 13(9):897–903.
68 Xiao M, et al. (2014) A fast deposition-crystallization procedure for highly efficient lead iodide perovskite thin-film solar cells. *Angew Chem Int Ed* 53(37): 9898–9903.
69 Schmidt LC, et al. (2014) Nontemplate synthesis of $CH_3NH_3PbBr_3$ perovskite nanoparticles. *J Am Chem Soc* 136(3):850–853.
70 Gonzalez-Carrero S, Galian RE, Pérez-Prieto J (2015) Maximizing the emissive properties of $CH_3NH_3PbBr_3$ perovskite nanoparticles. *J Mater Chem A* 3(17): 9187–9193.
71 Zhang F, et al. (2015) Brightly luminescent and color-tunable colloidal $CH_3NH_3PbX_3$ (X = Br, I, Cl) quantum dots: Potential alternatives for display technology. *ACS Nano* 9(4):4533–4542.
72 Huang H, Susha AS, Kershaw SV, Hung TF, Rogach AL (2015) Control of emission color of high quantum yield $CH_3NH_3PbBr_3$ perovskite quantum dots by precipitation temperature. *Adv Sci* 2(9):1500194.
73 Tachikawa T, Karimata I, Kobori Y (2015) Surface charge trapping in organolead halide perovskites explored by single-particle photoluminescence imaging. *J Phys Chem Lett* 6(16):3195–3201.
74 Zheng K, et al. (2015) Exciton binding energy and the nature of emissive states in organometal halide perovskites. *J Phys Chem Lett* 6(15):2969–2975.
75 Kollek T, et al. (2015) Porous and shape-anisotropic single crystals of the semiconductor perovskite $CH_3NH_3PbI_3$ from a single-source precursor. *Angew Chem Int Ed* 54(4):1341–1346.
76 Koolyk M, Amgar D, Aharon S, Etgar L (2016) Kinetics of cesium lead halide perovskite nanoparticle growth; focusing and de-focusing of size distribution. *Nanoscale* 8(12):6403–6409.
77 Song J, et al. (2015) Quantum dot light-emitting diodes based on inorganic perovskite cesium lead halides ($CsPbX_3$). *Adv Mater* 27(44):7162–7167.
78 Li X, et al. (2016) $CsPbX_3$ quantum dots for lighting and displays: Room-temperature synthesis, photoluminescence superiorities, underlying origins and white light-emitting diodes. *Adv Funct Mater* 26(15):2435–2445.
79 Aygüler MF, et al. (2015) Light-emitting electrochemical cells based on hybrid lead halide perovskite nanoparticles. *J Phys Chem C* 119(21):12047–12054.
80 Zhang X, et al. (2016) Enhancing the brightness of cesium lead halide perovskite nanocrystal based green light-emitting devices through the interface engineering with perfluorinated ionomer. *Nano Lett* 16(2):1415–1420.
81 Ling Y, et al. (2016) Bright light-emitting diodes based on organometal halide perovskite nanoplatelets. *Adv Mater* 28(2):305–311.
82 Li G, et al. (2016) Highly efficient perovskite nanocrystal light-emitting diodes enabled by a universal crosslinking method. *Adv Mater* 28(18):3528–3534.
83 Tian Y, et al. (2015) Giant photoluminescence blinking of perovskite nanocrystals reveals single-trap control of luminescence. *Nano Lett* 15(3):1603–1608.
84 Galisteo-López JF, Anaya M, Calvo ME, Míguez H (2015) Environmental effects on the photophysics of organic–inorganic halide perovskites. *J Phys Chem Lett* 6(12):2200–2205.
85 Makarov NS, et al. (2016) Spectral and dynamical properties of single excitons, biexcitons, and trions in cesium–lead-halide perovskite quantum dots. *Nano Lett* 16(4):2349–2362.
86 Sapori D, Kepenekian M, Pedesseau L, Katan C, Even J (2016) Quantum confinement and dielectric profiles of colloidal nanoplatelets of halide inorganic and hybrid organic-inorganic perovskites. *Nanoscale* 8(12):6369–6378.
87 Saxena K, Jain VK, Mehta DS (2009) A review on the light extraction techniques in organic electroluminescent devices. *Opt Mater* 32(1):221–233.
88 Galkowski K, et al. (2016) Determination of the exciton binding energy and effective masses for methylammonium and formamidinium lead tri-halide perovskite semiconductors. *Energy Environ Sci* 9(3):962–970.
89 Heo JH, Song DH, Im SH (2014) Planar $CH_3NH_3PbBr_3$ hybrid solar cells with 10.4% power conversion efficiency, fabricated by controlled crystallization in the spin-coating process. *Adv Mater* 26(48):8179–8183.
90 Gong X, et al. (2016) Highly efficient quantum dot near-infrared light-emitting diodes. *Nat Photonics* 10(4):253–257.
91 Ning Z, et al. (2015) Quantum-dot-in-perovskite solids. *Nature* 523(7560):324–328.
92 Anaya M, et al. (2016) Optical analysis of $CH_3NH_3Sn_xPb_{1-x}I_3$ absorbers: A roadmap for perovskite-on-perovskite tandem solar cells. *J Mater Chem A* 4(29): 11214–11221.
93 Saliba M, et al. (2016) Structured organic–inorganic perovskite toward a distributed feedback laser. *Adv Mater* 28(5):923–929.
94 Meerheim R, Furno M, Hofmann S, Lüssem B, Leo K (2010) Quantification of energy loss mechanisms in organic light-emitting diodes. *Appl Phys Lett* 97(25): 253305.
95 Liu J, et al. (2016) Two-dimensional $CH_3NH_3PbI_3$ perovskite: Synthesis and optoelectronic application. *ACS Nano* 10(3):3536–3542.
96 Dou L, et al. (2015) Atomically thin two-dimensional organic-inorganic hybrid perovskites. *Science* 349(6255):1518–1521.